Mobile LiDAR Scanner

M. Cuesta[1], D. Dolorfino[2], A. M. Jimenez[1], T. Morgan[2]

CREOL, College of Optics and Photonics[1]

Dept. of Electrical Computer Engineering[2]

University of Central Florida, Orlando, Florida 32816, USA

***Abstract*—Reconnaissance is necessary to most military efforts as information is increasingly becoming a crucial asset in modern warfare. Remote monitoring of dangerous areas prior to troops engaging can reduce the number of casualties and aid our soldiers in accomplishing their missions more effectively. For our project we are designing an entire LiDAR scanning system that will render a 3D image of the scanned area. The project's most unique feature is the variable field of view. By having a field of view that can be used defined depending on the user defined scanning distance. This allows us to obtain the best axial resolution for each rendered scan.**

Key terms - Optical reflection, point cloud compression, laser radar, optical modulation, integrated optics, protocols.

I. Introduction

LiDAR, which stands for Light Detection and Ranging, is a method of remote sensing that uses lasers to measure distances. The reflected light from the target can be stored and processed to produce a 3-dimensional model of the area. LiDAR differentiates from conventional remote sensing due to the fact that it uses light in the near and mid-infrared sections of the electromagnetic spectrum (NIR/MIR). LiDAR technology is also capable of working in low ambient light settings, over long ranges depending on the optical setup, and can represent both stationary and moving objects.

The goal of this project is to create a remote-control car fitted with a LiDAR scanning system on top. With this configuration, we want to be able to drive the remote-controlled or RC car into a room and produce a 3-dimensional model of that room. This idea was suggested because recon in the military can be a dangerous job. To make it easier on our soldiers and to keep them safe, we plan on creating a device that goes into enclosed areas and scans using LiDAR technology. The data from the scans are sent via a wireless connection to a remote user interface. The data is then processed to produce a 3-dimensional model of the area.

The scan would begin to take a series of images using the epc635 CCD sensor, outputting DCS frames that would be processed into 3D ToF images. These images are passed back to the host computer where it is processed into a point-cloud representation. The proposal came from understanding the harsh situations military soldiers have to deal with when performing reconnaissance in a room or area. One deems a room to be dangerous before entering if the soldier does not know what can be on the opposite side of the door. This scanner can also be applied for exploratory endeavors, to avoid risk of human life.

In this paper we will discuss the design approach taken by the group for individual subsections as well as the integration of subsystems to create the Mobile LiDAR Scanner.

II. Illumination System

The illumination subsystem is a crucial component of the LiDAR. Several considerations must be made when designing this subsystem, including type of emitter, emission wavelength, optical design and light modulation. In addition to these, the Mobile LiDAR scanner illumination system seeks to optimize illumination of the target, thus other factors like tilting angle of the illumination system and illumination field of view (FOV) were also considered.

A. Emitter Selection

The emitter chosen was an EGA2000 high power VCSEL from AMS with a narrow emission line width of 8nm, a maximum output power of 4.3 W and a vertical FOV of 58°. The narrow bandwidth improves the SNR if a band-pass filter is used for the detector, the high power allows for detection of farther objects well as objects with lower reflectivity. The wide FOV was managed with the optical system. Moreover, VCSELs can typically be directly modulated at faster frequencies than EELs, which, as will be later discussed, allows for obtaining better resolution of the time-of-flight (ToF) measurements.

B. Wavelength Selection

The EGA2000 has its emission peak at 940 nm which is a standard wavelength for ToF measurements. This wavelength corresponds to a low emission line for solar radiation at ground, which is favorable for outdoor applications. In addition, attenuation due to humidity is diminished at 940 nm. A downside is an increased risk of damage to the eye. Maintaining low intensities for short-distance measurements and keeping the beam low (<50cm from the ground) for long-distance measurements can decrease this risk.

C. Optics

A variable FOV optical system is achieved with a zoom-lens-like design using cylindrical lenses to vary the vertical vergence of the outgoing beam from nearly collimated light at approximately 4 mm in diameter to a beam with 45° angle of divergence. The adjustable cylindrical lens is translated across the optical axis by a small stepper motor to vary the FOV. Fig. 1 shows the minimum and maximum possible FOVs with this system. Out of the four lenses, all are standard and three are AR coated for NIR light. From nonsequential simulations, the maximum expected power loss through the entire system is 15%. This could be reduced by employing only coated lenses which would require customized lens manufacturing for the design values presented in Fig. 2. The values with unspecified units are in millimeters. This design is highly sensitive to collimation, as even small changes of a few tenths of a millimeter can highly affect the output FOV. Therefore, the collimation lens position must be precisely adjusted with a micrometer to the specified value in Fig. 2.

D. Modulating the VCSEL

To measure the distance of the target, the LiDAR system measures the time shift between the outgoing pulse train of the VCSEL and the incoming pulse train detected. Consequently, the

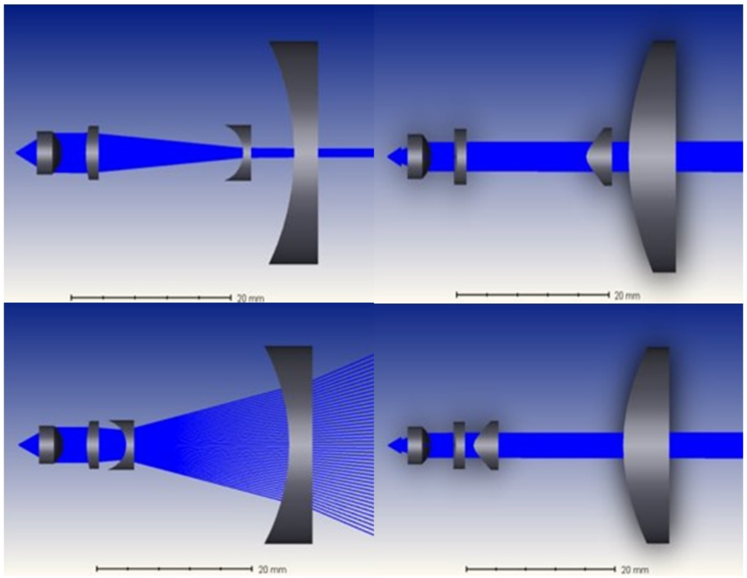

Figure 1. Horizontal and Vertical FOVs for Maximum and Minimum Configurations. The two images on the left depict the side profile of the illumination optics while the two images on the right depict a top down view of the illumination optics. In this configuration, we can see that there is no lateral change to the profile of the beam in the x-direction but only an expansion and constriction in the y-direction. This will allow us to illuminate the object space with a fan and collect and capture that light onto the sensor.

Lens Type	Edmund Part #	R1	R2	Position from VCSEL	Center Thickness	Material	Coating	Diameter
Aspheric	87158	Infinity	-2.684	0.840	3.135	D-ZK3	600-1050 nm	6.00
Cylindrical	69742	12.403	Infinity	6.975	1.60	N-BK7	600-1050 nm	6.00
Cylindrical	46191	-3.240	Infinity	12.075-26.575	1.00	BK7	--	6.25
Cylindrical	69823	-25.930	Infinity	32.075	3.00	N-BK7	600-1050 nm	25.00

Figure 2. Prescription table for the illumination optics for the Mobile LiDAR Scanner.

modulation of the illumination light is extremely important, as its frequency determines the maximum unambiguous detectable distance, and the pulse width or duty cycle determines the axial resolution. In a simplistic approach, the axial resolution can be calculated as in eq. 1 where Δt is the pulse width or D/f_{mod} (D is the duty cycle, f_{mod} is the modulation frequency). Replacing Δt for $t = 1/f_{mod}$ gives the unambiguity distance.

$$\Delta d = \Delta t \frac{c}{2}. \tag{1}$$

Given that the minimum specified distance to be detected is 1 m, the corresponding time delay is approximately 6.67 ns. To reduce noise and increase precision when measuring the phase shift between the modulation and demodulation waves, $1/f_{mod}$ should not be greater than $100\Delta T$ where ΔT is the time phase shift to be measured. This a completely arbitrary value that was established for the particular system discussed here. As such, the minimum modulation frequency required for detection at 1m is 1.5 MHz.

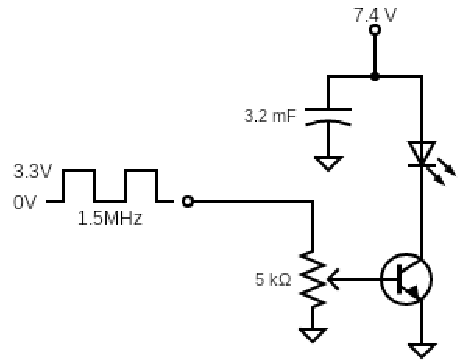

Figure 3. VCSEL Driver with NPN Switching Transistor and Digital Potentiomete.r

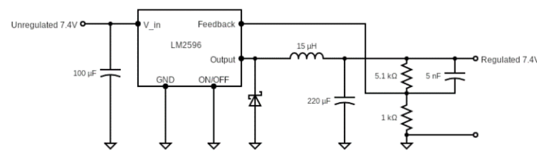

Figure 4. Voltage Regulation Circuit for VCSEL Power Supply.

The VCSEL driver circuit must provide short rising and fall times to achieve high modulation frequencies, as well as modulate high currents of up to 2A to provide high intensities of light. A simple transistor-based switching circuit can work for the moderately high frequencies required. The circuit shown in Fig. 2 shows an NPN transistor switched by a 3.3V positive clock and a voltage supply of 7.4V. The modulation clock goes through a digital potentiometer in a voltage divider configuration with the wiper connected to the base of the transistor. By changing the position of the wiper, the switching voltage is varied, effectively changing the collector-to-emitter VCE voltage and therefore the voltage across the VCSEL. In this way the light intensity can be controlled. The supply voltage of 7.4V is regulated by the circuit shown in Fig. 4 using a switching buck converter to maintain the voltage from a 7.7V battery steady throughout time and during modulation.

This driver circuit design, while simple, has several drawbacks. Firstly, the position of the potentiometer makes it the limiting factor for modulation. While the NPN transistor can go up to 5MHz while maintaining decent gain and pulse stability, typical potentiometers are rated at only a few hundreds of kilohertz. Changing the position of the potentiometer to replace the 5 KΩ resistor in the voltage regulation circuit would allow to control the current through the VCSEL more effectively without affecting the modulation frequency. Secondly, the transistor has comparable resistance to that of the VCSEL during the ON state, and therefore consumes some of the power reducing the maximum current that can be achieved. A power N-Channel MOSFET with low ON resistance would be a more appropriate choice to modulate the VCSEL in parallel to the source-drain voltage. Fig. 5 shows a recommended circuit from Texas Instrument (TI) to modulate high-

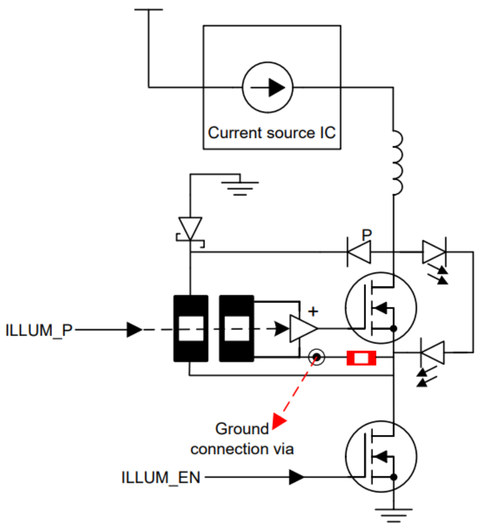

Figure 5. In this figure we show a recommended circuit from Texas Instruments on how to modulate a VCSEL or laser diode at high frequencies.

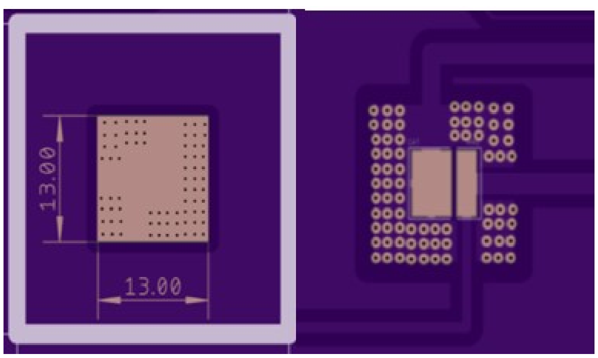

Figure 6. VCSEL Pads on PCB with Isolated Plane and Heatsink for Heat Dissipation.

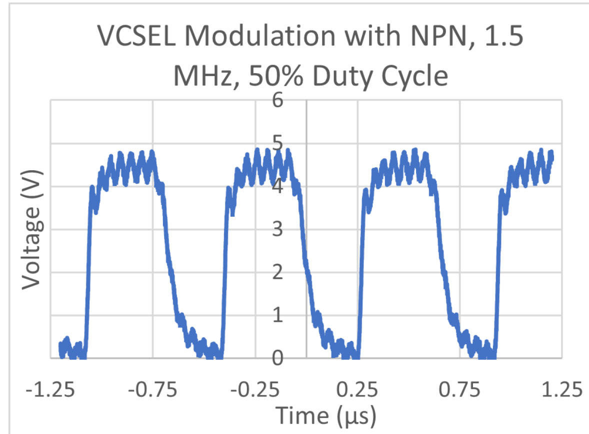

Figure 7. Voltage across VCSEL when switching NPN transistor with 3.3 V positive clock at 1.5Mhz with 50% duty cycle.

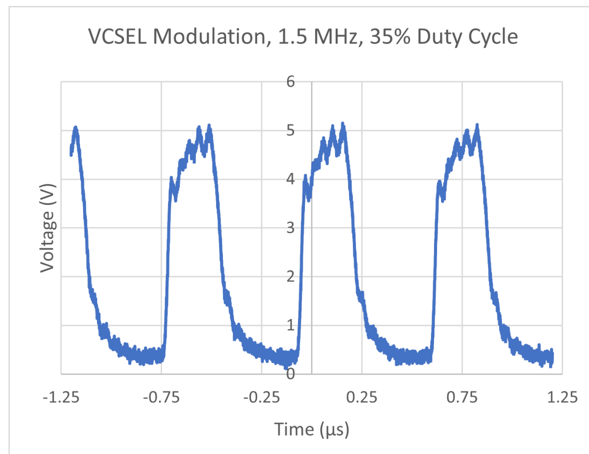

Figure 8. Voltage across VCSEL when switching NPN transistor with 3.3 V positive clock at 1.5Mhz with 35% duty cycle.

power VCSELs at high frequencies [1]. This circuit could be potentially used as an alternative to that shown in Fig. 3.

When driving the VCSEL at currents as high as 2 A, it is important to control the temperature. Fig. 6 shows the PCB design for the VCSEL pads. A plane connected to the VCSEL cathode is created isolated from the ground plane. Vias are placed to help the heat dissipation from the bottom of the board where the VCSEL is soldered to the top of the board where the copper is exposed to connect a heat sink.

E. VCSEL Modulation

When modulating the VCSEL with the circuit shown in Fig. 3, the voltage across the VCSEL is as shown in Fig. 7. There is an average maximum voltage of approximately 4.5V with a considerable ripple likely caused by parasitic inductances and voltages of the circuit. This ripple could be minimized by adding appropriate capacitors to filter out the noise. Bandwidth limitations of the transistor also increase the ripple at high frequencies. In addition, the voltage does not drop quick enough and extends the pulse width. Fig. 8 shows that by reducing the duty cycle, the pulse width can be appropriately reduced to compensate for this.

III. Detection System

The detection system of the Mobile LiDAR Scanner can be simplified into three distinct subsections: the sensor, the optics, and the power distribution. The most important consideration for selecting a sensor is the response time and responsivity at the desired wavelength. For our project we had initially selected the EPC 635 CCD TOF Sensor. This product was selected over a photodiode array due to the fast response time and responsivity at our desired wavelength. The EPC 635 CCD TOF Sensor allowed us to select different modes of operations for different purposes while maintaining the most optimal resolution.

A. Detection Optics

For designing the collection optics for the Mobile LiDAR Scanner, we needed to create a fast system so due to the small effective focal length that we calculated, a fast optical system is one with a low F/. Within the present design the group selected to use a 20 nm FWHM bandpass filter centered at the operating wavelength of 940 nm. Fig. 9 is the optical prescription for the detection system of the Mobile LiDAR Scanner. Due to budget constraints the collection

		Surface Type	Radius	Thickness	Material	Coating
0	OBJECT	Standard	Infinity	Infinity		
1		Standard	Infinity	10.000		
2	(aper)	Standard	Infinity	3.500	N-BK7	
3		Standard	Infinity	0.500		
4	STOP (aper)	Standard	8.880	2.380	N-BK7	EO_NIRII_517
5	(aper)	Standard	-8.880	0.000		EO_NIRII_517
6	(aper)	Standard	Infinity	1.500	N-SF11	EO_NIRII_785
7	(aper)	Standard	4.710	0.650		EO_NIRII_785
8	(aper)	Standard	6.580	2.600	N-LASF...	
9	(aper)	Standard	-6.580	0.439		
12	(aper)	Standard	6.580	2.600	N-LASF...	
13	(aper)	Standard	-6.580	0.800		
14	IMAGE	Standard	Infinity	-		

Figure 9. Optical prescription for the detection optics of the Mobile LiDAR Scanner. This design features entirely off the shelf optics due to the budget and time restrictions that personalized optics presents. The optics of our project are to scale with the active region of the sensor, this is so we can have a physical aperture of lens diameter relative to the size of the sensor.

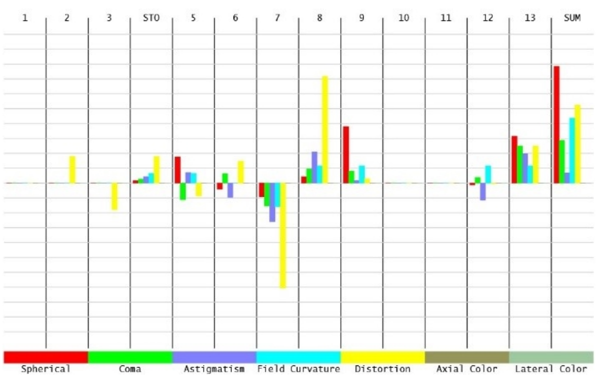

Figure 10. Seidel diagram for the collection optics. In this diagram we see the contribution of the primary third order aberrations to our system, where the most prominent are spherical aberration and distortion. From the diagram above we can clearly see that surfaces 8/9 and 12/13 are the largest contributors to the aberrations of the entire system. These four surfaces make up the last two lenses of the system whose purpose is to decrease the height of the image such that it is fully incident on the active region of the EPC 635 CCD TOF sensor.

optics needed to be off the shelf products which meant that we needed to design a generalized system that would be capable of obtaining the best image while minimizing aberrations as much as possible. The aberrations that we opted to minimize for the collection optics were astigmatism, coma, and field curvature. For the purpose of detecting distances to generate a point cloud, it is crucial that we are able to focus the most amount of light onto individual pixels on our sensor.

In Fig. 10, we see the Seidel diagram for our detection optics. In this figure we see that the most prominent aberration is spherical aberration which is inability for rays to focus on the paraxial focal point of the system. This is our largest aberration because we needed to intentionally deviate from the paraxial focal point for the on-axis rays to compensate for the field curvature experienced by the largest incoming ray angles. The second most prominent aberration of the system is distortion, which is where the image plane is skewed. Since the purpose of our project is to detect distances rather than displaying an image, we are able to afford more distortion as it does not affect the purpose of the Mobile

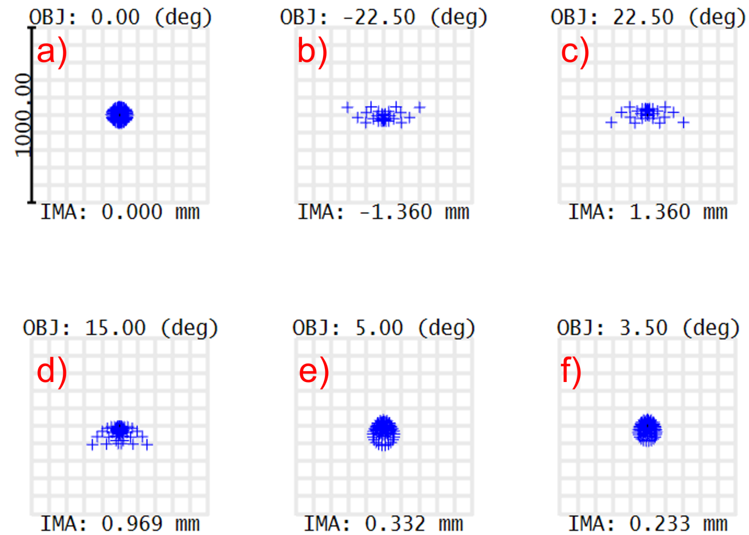

Figure 11. Spot diagram for incoming light at half angles from the optical axis. The EPC 635 CCD TOF Sensor has an active pixel area of 160 × 60 pixels, where each pixel has an area of 20μm x 20μm. a) On axis rays with an RMS spot size of 38.937μm. b c) spot size that equate to the entire 45° FOV with an RMS spot size of 75.895μm. d, e, f) Intermediate half angles within the 45° FOV to show the progression of RMS spot size.

LiDAR Scanner.

The detection optics were designed in a manner such that the optics would be able to collect light from a field of view of 45°. The EPC 635 CCD TOF Sensor has an active pixel region of 160 × 60 pixels, where each pixel has an area of 20μm × 20μm. The design goal for the detection optics was to be able to focus the light down into one individual pixel, such that there is a 1:1 correlation between a point in the object space to a pixel in the image space. Ideally, this would allow us to have a large resolution because each individual point of reflection in the image space corresponds to an individual pixel which represents a single point within our point cloud.

Fig. 11 shows the spot diagram for the focused rays with a half angle FOV of up to 45°. Due to the imperfections of our optical system and the present aberrations, the RMS spot size of the focused light onto the sensor is larger than the area of an individual pixel, this results in a pixel blur that has to be accounted for in the software image processing. The RMS spot size radius of the 0° and 22.5° are 38.937 μm and 75.895 μm respectively.

From Fig. 11, it is clear that the maximum pixel blur is approximately 8 pixels and occurs at the 22.5° FOV. Since we know the beam profile of is a vertical slit and the collected light will be incident there, then it is helpful to filter out the unactive pixel region on the sensor. This will allow us to eliminate irrelevant data as well as background noise. This feature is programmable on the EPC 635 CCD TOF Sensor.

In order to integrate the detection optics into the Mobile LiDAR Scanner, we designed specific optical mounts that hold the lenses in place while maintaining the optical axis on the center of the optics as well as aligning it to the center of the EPC 635 CCD TOF sensor. The optical mounts are printed with PLA filament, Polylactic Acid filament. PLA filaments have been shown to be quite resistive to

Pin	Voltage	Ripple
V_{DDIO}	+ 2.5 / + 3.3 V	± 50 mV
V_{DD}/V_{DDPLL}	+ 1.8 V	± 20 mV
V_{DDA}	+ 5.0 V	± 20 mV
V_{DDPXH}	+ 10.0 V	± 20 mV
V_{BS}	- 10.0 V	± 50 mV

Figure 12. Voltage requirements for powering on the EPC 635 CCD TOF sensor. These voltages must be applied sequentially, where VDDIO and VDD/VDDPLL get applied first followed by VDDA and VDDPXH and finally by VBS. After all of the voltages have been applied RESET so that the internal oscillator clocks can reach their operating frequencies before normal operation can be reached.

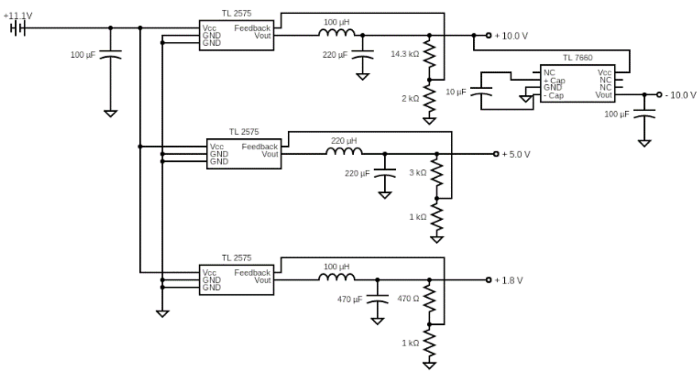

Figure 13. Power Circuit for the EPC 635 CCD TOF sensor. In this circuit we utilize a + 11.1 V / 800 mAh battery as our DC supply, and step down this voltage to +10.0 V, + 5.0 V, and + 1.8 V through a TL 2575 step down voltage regulator. The + 10.0 V are then passed through the TL 7660 voltage inverter to obtain the -10.0 V required by the CCD sensor. When measured on an oscilloscope the TL 2575 eliminates the ripple voltage allowing for a stable supply to the EPC 635 CCD TOF sensor.

impacts and tensile strength. Due to its high resistivity to impact, the group can be confident that this material will keep the optical components in place while moving. For printing, the group will use the Original Prusa i3 machine. Since the Mobile LiDAR Scanner requires very high precision for the optical components, the group requires a machine that can print details in the millimeter regime. The Original Prusa i3 machine is capable to print details with 0.05 - 0.35 mm precision.

B. CCD Sensor Circuitry

When working with the EPC 635 CCD TOF sensor, five distinct voltages must be applied to power on the internal circuitry, clocks, and photodiode array. Fig. 12, shows the corresponding voltages to be supplied to each individual pin as well as the ripple tolerance that can be sustained at each. To integrate the EPC 635 CCD TOF Sensor into our LiDAR module, we designed a power distribution board for the sensor that correctly distributes the necessary power to the sensor. Fig. 13, is the schematic for the circuitry used to achieve the required voltage specifications from a single 11.1 V battery and from the BeagleBone Black + 3.3 V supply pin. From the schematic in Fig. 13, we use the TL 2575 Step down buck converter to allow us to get a regulated output voltage. The TL 2575 was the selected step down buck converted because for an 11.1 V input with 800 mA the efficiency is approximately 80% at a 5 V output with increasing efficiency the closer the step down is to the input voltage and decreasing up to 75% for the 1.8 V output. From Fig. 12, our power circuit must minimize the output ripple voltage to meat the required levels provided by ESPROS Photonics for powering on the EPC 635 CCD TOF Sensor. The output capacitors for each power pin are selected specifically to maintain the ripple voltage at 1% of 11.1 V input. The TL 2575 step down buck converter is capable of providing an adjustable output voltage through the following equation,

$$V_{out} = 1.23(1 - \frac{R_2}{R_1}). \tag{2}$$

The adjustable output is independent of the input voltage and solely dependent on the output resistors R1 and R2. The inductors of the power circuit are placed there to ensure that the buck converter is always operating in continuous mode, when applying a heavy load current, the inductor allows for the continuous flow of. The inductors that have been selected for this circuit are rated at a current slightly higher than our operating current to avoid saturation. The battery of our project provides 800 mAh, although during the stress test for the power circuit the current did not increase above 70 mA even during image acquisition.

IV. Hardware

A. BeagleBone Black

The BeagleBone Black (or BBB) is a community supported and low-cost, system on chip (SoC), developmental platform that provides adequate computational power to modulate the VCSEL driver, control the CCD sensor, and interpret the user input for motor movement. The BBB uses a AM335x 1 GHz ARM Cortex-A8 processor with 512 MB of DDR3 RAM, 4GB 8-bit eMMC flash storage and 2 PRU 32-bit microcontrollers. The BBB runs on Linux and has the latest Debian image flashed on to it. It is also software compatible with Android and Ubuntu to name a few. This mini-computer also come with many peripheral connectivity ports such as: USB client for power and communication, Ethernet to connect to the internet, HDMI and 92 pin headers that are compatible with different communication protocols, power externally and using the pins to control slave devices. Fig. 14 shows how the BBB interacts with different parts of the system.

To ensure the BBB functions the way we intend, flashing Linux and installing essential libraries aided in the development of this system. To properly install the dependencies, a micro-SD card with the correct image needed to be flashed to the BBB initially. Following the case of the image being flashed, connecting to the internet was vital in receiving the necessary libraries.

Cloud9 is the IDE associated with this device, after applying 5V power either by the USB connection from a laptop/computer or a 5V DC input, the BBB creates a DCHP server to SSH into and gain access to its software. In this software gives us the ability to implement the way we see fit, whether it's writing programs to have the BBB operate uniquely on specific pins, or even setting the BBB up in a way that changes the way it processes data. The flexibility it possess gives us different functionalities.

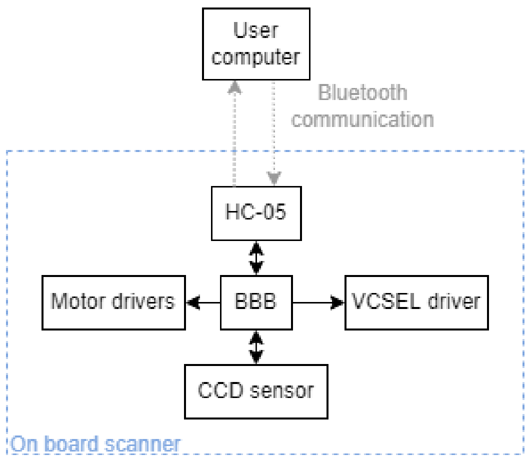

Figure 14. This block diagram shows where the BBB will fit in the overall system. It acts as the heart of the Mobile LiDAR Scanner, taking care of the motor drivers, CCD sensor and custom VCSEL driver.

B. Bluetooth

Wireless communications must be established between the Mobile LiDAR Scanner and the host computer used to generate the point-cloud presentation of the ToF image and send commands. The Bluetooth module that we decided to use was DSD Tech's HC-05 Bluetooth module.

The HC-05 Bluetooth module supports Bluetooth 2.0, allowing it to communicate with most Bluetooth-enabled laptops. This module was chosen for its ability to act as both master and slave mode. The HC-05 simple interface that allows to integrate into most microcontroller systems that use UART. The TX pin was connected to the RXD pin of the UART channel 4 of the BBB. The RX pin of the HC-05 was connected to a voltage divider which lower the voltage level from the TXD pin from the BBB. Fig. 17 shows how the module and BBB are implemented to interpret keyboard input into motor movement.

C. Communication protocols

UART, or Universal Asynchronous Receiver and Transmitter, is the interface used to transmit data between the Mobile LiDAR Scanner and the host computer. The HC-05 Bluetooth module acted as a medium for this transmission. The movement for the Mobile LiDAR scanner is not done simultaneously as the scanning. It only needs to react to the input given from the user. Thus, the asynchronous nature of the UART was ideal for this communication.

I2C, or Inter-integrated Communication, was extensively used to configure the CCD sensor. This bus topology of this protocol allows multiple peripherals to be connected to a single set of wires, serial clock (SCK) and serial data (SDA), controlled by a single controller. In the case of project, the BBB acts as the master and the CCD sensor acts as the slave.

SPI, or Serial Peripheral Interface, is the last communication protocol use in this project. This protocol was used to send commands to the potentiometer on the VCSEL laser driver PCB. Only the pin SI (serial in) is used with this potentiometer, thus a SO (serial out) pin was not necessary. However, in our final design, we found that potentiometer could just be replaced with a resistor, meaning SPI would not be needed for the laser driver PCB. However, we found that we could use SPI for an alternative data retrieval method for the CCD sensor. This is discussed in Sec. V-A.

D. Motors and motor drivers

In total there are six distinct motors that must be driven. Two of the motors are direct current and four others are all bipoloar stepper motors. The two DC motors are used for the locomotion of the Mobile LiDAR Scanner, driving the sprockets on the belted wheels. The rotation motor is a Nema 17 Stepper motor by Usongshine. This motor will be used to spin our custom LiDAR system, allow it to capture back multiple images of the area and keep track of its current angle. The tilting motor and FoV tuning motors were repurposed stepper motors with lead screws from an old computer. We soldered wires to the four polarity pins on each of the three motors. These polarity pins are interfaced onto an A4988 stepper motor driver.

Two different motor drivers were used to interface with the motors on our Mobile LiDAR scanner: L298N and A4998. The L298N is a dual H-Bridge motor driver IC (integrated circuit). This rated with a power supply of 5-35 V DC and can control two DC motors up to 2 A. It can also be used to interface bipolar stepper motors as well. Two L298N drivers are used to drive the DC motors and the rotation motor.

The A4988 motor is micro-stepping motor driver that has a built in translator that allows for 2 pins (step and direction) to control the movement rather than 4. We use these motor drivers to drive our stepper motors above on top of the rotating platform, the tilting motor and the FoV motors.

V. Software

For our project, our team decided to code in Python. Python is a widely used high-level programming language. It also has may libraries that can be useful to build the programs that control our Mobile LiDAR Scanner and the host computer.

Data processing in this system is used in a unique way. From capturing the image on the CCD sensor and transferring that data via USB, the raw data from the image would be rendered and formatted on a host computer to create a faster compilation time. The optimal way of performing this to limit the amount of work done by the BeagleBone Black.

For the purpose of this presentation, the team will be showcasing the Mobile LiDAR Scanner able to process one ToF image into a point-cloud representation. The team is currently limited by the insufficient sampling time of the BBB's GPIOs and the rendering limit of OpenGL.

A. Interfacing the CCD sensor

The CCD sensor was the most complex portion of this project. Receiving all valid data bytes from each pixel was a challenge. Nonetheless, interfacing the data was quite simple.

With our custom power circuit, the CCD sensor was able to be turned on and seen as a device on address 0x20 on the BBB. Using the I2C interface on the CCD sensor, the BBB can configure settings for the shot and start the shutter. For our project, the CCD sensor is configured to take a single shot, outputting 4 DCS frames for 1 ToF measurement. To start the image acquisition, a software shutter is used. This is done by flipping bit 0 on register 0xA4 on the I2C interface. The configuration of the shot is set up by writing values to the registers.

Currently, the data that has been procured by the BBB is not sufficient to calculate a ToF image. Using our I2C configuration, we are expecting 4 DCS frames-worth of data, totaling 38,912 bytes of pure pixel data. In addition, 4-byte "labels" are also injected into the data to denote when a DCS frame starts/ends and where lines of pixels start/end. In current tests, the BBB has been able to capture about 70 bytes of data. The main issue is timing between the BBB and CCD sensor. We slowed the DCLK to its slowest rate, 2.5 MHz, but the BBB can sample a very small portion of the 4 DCS frames. The data for all frames are needed to calculate the ToF image.

For an alternative approach, the group has looked into using the TI's MSP430FR6989 LaunchPad Development Kit as a buffer to collect pixel data from the CCD sensor. In terms of SPI communication protocol, the BBB would act as the slave and the MSP430 would act as master transferring data in a half duplex mode. Instead of collecting the data directly from the CCD sensor to the BBB's data pins, which could cause delay upon receiving data bits, the MSP430 could act as an immediate buffer to store incoming data, then transfer the pixel data via SPI. In terms of the hardware implementation, the data pins (DATA[7:0]) from the CCD sensor are routed directly to the MSP430 alongside SHUTTER and DCLK. The SHUTTER pin is toggled, sending a hardware shutter signal to the CCD sensor, starting image acquisition. On the the rising edge of the DCLK, DATA[7:0] bytes are written to the memory of the MSP430, resulting in around 39k bytes for 4 DCS frames for 1 ToF measurement. This is okay since the MSP430 has an FRAM of 128kB. While using the Development Kit is not ideal for the final design, it allows us to collect all of the DCS frame data from the CCD sensor that are used to build the final ToF image.

B. *Image processing and point cloud generation*

Essentially, the data used that's transferred to the host computer would transmit the data to become readable, from there it would transmit to a form of light intensity and the would be used to depict a distance using OpenGL and *pygame*. Fig. 15 visually depicts sample data that we created by the group to show depth perception of through OpenGL and *pygame*.

In order to transmit data between the host computer, we originally planned to have a Python program flashed on the BBB which would take input from the user's computer using UART. In movement mode, the keyboard input would be used to move the Mobile LiDAR Scanner. Once in the desired position, the user can exit and go into scanning mode. During scanning the mode, the scanner takes ToF measurements and transmits the information through Bluetooth to the users computer for data processing and image rendering.

After synchronizing the clocks, and shutter was enabled, the program written captures the incoming DCS frames byte by byte. The DCS frames are transferred to the host computer where they are

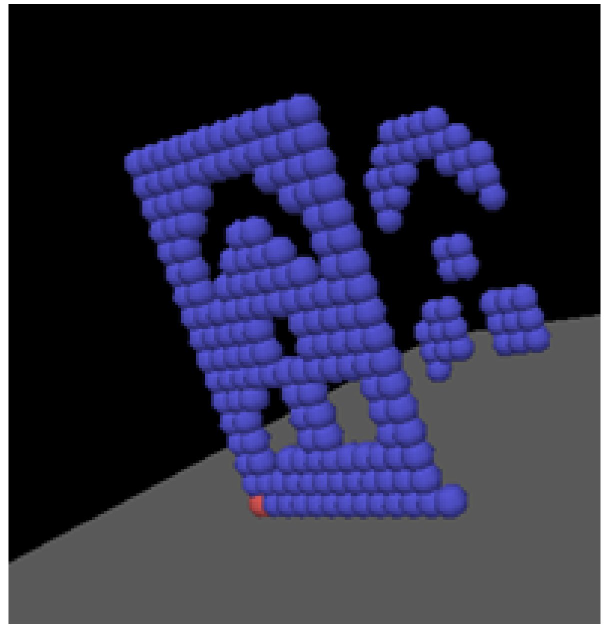

Figure 15. 3-dimensional point cloud data representation with OpenGL and *pygame*. This software allows one to display depths and distances while being able to maneuver through the point cloud data. The following image is sample data that was create to show how two objects that lie in the same plane can have different distances and hence a perception of depth created by OpenGL.

```
for i in range(9000):
        if(beg == 1):
                if (i % 160 == 0):
                        x = x + 0.1
                        z = z - 16
                        begs = 1
        if (sta == 0):
                glTranslatef(-1, int(arr[i])*0.1, 0)
                glColor4f(0.5, 0.2, 0.2, 1)
                gluSphere(sphere, 0.07, 10, 4)
        if (sta == 1):
                glTranslatef(x, ((int(arr[i-1]) - int(arr[i]))*0.1), z)
                glColor4f(0.2, 0.2, 0.5, 1)
                gluSphere(sphere, 0.07, 10, 4)
        if(begs == 1):
                z = 0.1
                x = 0
        beg = 1
        sta = 1
        begs = 0
```

Figure 16. Python code representing the heart of plotting distance points in OpenGL

calculated to create the ToF image. The ToF image bytes are then written to a file, containing 9,600 bytes from the 160 x 60 active pixel region. Depending on the light intensity of the image, we developed a program in OpenGL to display the distance measured from each pixel. Depending on the intensity of the light returned from each pixel resulted in the point rendered in our 3D space to have depth. The higher the intensity of the pixel, the closer the image is displayed on the program. This runs efficiently more efficiently if light is displayed behind the system. Knowing how light works, the closer the target is to the light, the more light gets reflected, the farther the target, the less light reflected.

This simple for loop computes the data in a unique way, the range is 9000 to symbolize the 160 x 60 pixels. The way in which OpenGL computes the distance associated with each point is it renders the first points position to initialize the setting of the rest of the points. The first "if" statement shows the initial point which would be referenced as (0,0) in a coordinate plane. glTranslate depicts the position whole glColor4f and gluSphere creates the color of the specific point and the size. To be able to plot 9000 points, the hallow spheres created with this function need to be created without executing large sphere. In the third function reference, the group decided to make the point 0.07 size. Therefore resulting in a complete program to plot 9000 points based on distance.

The second "if" statement in this block represents the points plotted for the rest of the distance pixels. Due to the nature of the glTranslate function, plotting the following points needed to be positioned based on the previous. Due to it associating it's position to the point before it, the math to plot distance was simply subtracting it to the referenced point then increasing/decreasing the distance based on how far it initially was. As shown in Fig 15, it correctly depicts it's distance.

To ensure this data would plot in a coordinate plane way, increasing the pointers for x, y and z were recorded and incremented accordingly with the variables "beg", "sta", and "begs". To conclude, this properly displays the reading gained from the CCD sensor to plot the light intensity for distance.

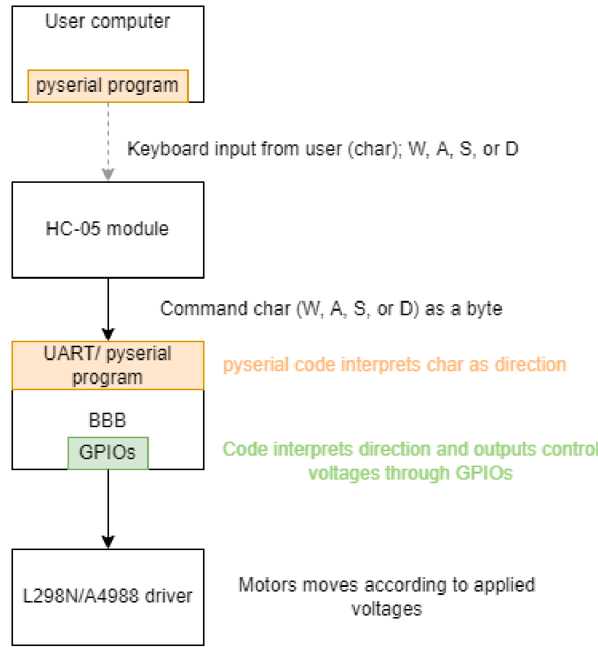

Figure 17. Flow chart showing how keyboard input from the user is processed into movement on the motors.

VI. Movement

Locomotion for the RC Platform is powered by a 7.4V battery which is routed to two DC gm25-370 motors. The two motors are connected to the L298N driver controller to manipulate the direction we wish to go in. The input pins located on the driver controller are routed to the BBB for logic input. With the proper connection established, the program written gives the user the ability to move in a desired location.

The movement is also interfaced with the HC-05 Bluetooth module for wireless control. *pyserial* for the Bluetooth module is the program applied to our application for sending and receiving bytes. This makes it easier for the user to gives specific directions to the RC Platform. The communication protocol used for the locomotion is UART. The full duplex mode gives the user faster data transmission when sending signals. We made it simple for the user, the keys 'w', 'a', 's', 'd', are well known keys to determine movement. By typing either of the keys, the direction associated with it will occur. Fig. 17 shows how the user input is translated into locomotion movement on the Mobile LiDAR Scanner.

In our testing, our team has been quite successful with implementing the locomotion, from host computer to motor movement, for our project quite early in the development. Using our what we learned with the locomotion motors, we were able to interface with each of the other stepper motors successfully even with a new motor driver.

VII. Conclusion

This two-semester long project gave the group an idea of the transition from an academic environment to an industry environment. This was the first exposure for the group members that gave them the opportunity to drive the project from an idea to the final product. Through this semester we learned how to work in a group setting with members of different academic backgrounds, conduct professional meetings and write professional documentation.

At the beginning of Senior Design 1, the group divided the responsibilities of the project based on the academic and technical background of each individual member as well as by the specific skills that each member wanted to learn. Throughout Senior Design 2, our group continued to work and support each other with each our responsibilities, each member contributing their best effort to the project. Among the successes and short-comings during our time in Senior Design, we hope take these precious lessons to heart as future engineers.

References

[1] T. Instruments. "Illumination Driving for Time of Flight Camera System." https://www.ti.com/lit/an/sbaa209b/sbaa209b.pdf?ts=1649100811143 (accessed 2022).

[2] E. P. Corporation. DATASHEET – epc635 3D TOF imager 160 x 60 pixel, ESPROS Photonics Corporation, EPC635 2020, p. 60. [Online]. Available: https://www.espros.com/downloads/01_Chips/Datasheet_epc635.pdf.

[3] "Bluetooth® Wireless Technology." Bluetooth SIG, Inc. https://www.bluetooth.com/learn-about-bluetooth/tech-overview/ (accessed November 2, 2021).

[4] T. Instruments. MSP430FR698x(1), MSP430FR598x(1) Mixed-Signal Microcontrollers, Texas Instruments 2018, p. 184. [Online]. Available: https://www.ti.com/lit/ds/symlink/msp430fr6989.pdf?ts=1638841159712

[5] W. E. e. G. C. KG. Infrared LED 940 nm 2018, p. 8. [Online]. Available: https://www.we-online.com/katalog/datasheet/15400394A3590.pdf.